

Cite this: DOI: 00.0000/xxxxxxxxxx

Electronic transport properties of MoS₂ nanoribbons embedded on butadiene solvent

Armando Pezo,^{*a,b} Matheus P. Lima,^c Marcio Costa,^a and Adalberto Fazzio^{*a}Received Date
Accepted Date

DOI: 00.0000/xxxxxxxxxx

Transition metal dichalcogenides (TMDCs) are promising materials for applications in nanoelectronics and correlated fields, where their metallic edge states play a fundamental role in the electronic transport. In this work, we investigate the transport properties of MoS₂ zigzag nanoribbons under a butadiene (C₄H₆) atmosphere, as this compound has been used to obtain MoS₂ flakes by exfoliation. We use the density functional theory combined to non-equilibrium Green's functions techniques, in a methodology contemplating disorder and different coverages. Our results indicate a strong modulation of the TMDC electronic transport properties driven by butadiene molecules anchored at their edges, producing the suppression of currents due to a backscattering process. Our results indicate a high sensibility of the TMDC edge states. Thus, the mechanisms used to reduce the dimensionality of MoS₂ considerably modify its transport properties.

1 Introduction

Graphene single layers were isolated a decade ago¹ challenging conjectures about the potential existence of two dimensional (2D) materials. This event initiated the 2D materials era². However, even with its remarkable properties, such as high charge carrier mobility³, mechanical stability⁴, thermal conductivity⁵, and interesting optical properties⁶, its practical use is not fully materialized. The existence of a gapless electronic spectrum near the Fermi level together with a difficulty for obtaining clean edges is a drawback for some applications. The so-called Klein tunneling, unconventional Hall effect, and anti-localization behavior are related to this feature⁷.

Following graphene, a profusion of 2D materials has been proposed and synthesized. Amongst them, the transition metal dichalcogenides (TMDC) occupies a special place. Its chemical formula MX_2 (M = transition metal, and X = S, Se, or Te) demonstrates the possibility of numerous distinct compositions with different characteristics^{8–10}. Furthermore, the crystal symmetry (2H, 1T or 1T') is another tuning parameter allowing to access semiconductor, metallic or topological insulator phases for some particular compositions^{11,12}. The study of other types of 2d layered materials was achieved by looking at the edges terminations and even exploring lateral heterostructures leading to interest-

ing results related to their I/V characteristics predicting negative differential resistance (NDR) features.^{13–18}. The broad variety of properties found in TMDCs together with the possibility of its control by several mechanisms opens the possibility of some promising technological applications, such as hydrodesulfurization catalyst¹⁹, thermoelectric devices²⁰, photovoltaic cells²¹, and nanotribology^{22,23}, just to mention a few. It's worth to mention that it's been argued that single(few) layer(s) MoS₂ could be used for logical electronic devices available to work at room temperature, being these thinner than the actual silicon-based films used in technological applications. The smaller dielectric constant with respect to that one of silicon is another advantage, leading to a less power consumption in transistors made of them. Measurements made on samples of this material at a bias of 500 mV gave a maximal on-current of 22 μ A (or 4.6 μ A/ μ m) at room temperature with a large I_{on}/I_{off} ratio higher than 10⁶ for a ± 4 V gate voltage range^{24,25}.

However, the integration of TMDCs in future technologies in many cases requests the reduction of its dimensionality. In this regard, the electronic properties of MoS₂ nanoribbons and nanoflakes are strongly constrained by their edge termination, whereas metallic and ferromagnetic edge states arise for the zigzag border. On the other hand, the armchair termination shows semiconducting and non-magnetic behavior, although it might transform into a metallic and magnetic under edge H-passivation^{22,26}.

There are several methods to reduce the dimensionality of MoS₂, ranging from chemical to mechanical routes^{12,27}. Recently, Gonçalves and coworkers used an assisted mechanical exfoliation to produce large MoS₂ flakes²⁸. They used a butadiene

^a Brazilian Nanotechnology National Laboratory (LNNano,CNPEN), Rua Giuseppe Máximo Scalfaro 10000, Campinas, SP 13083-970, Brazil; E-mail: armando.pezo@ufabc.edu.br; adalberto.fazzio@lnnano.cnpem.br

^b CCNH - Center for Natural Sciences and Humanities, Federal University of ABC, Santo André, SP, Brazil

^c Departamento de Física, Universidade Federal de São Carlos, 13565-905 São Carlos, São Paulo, Brasil

solution followed by an ultrasonication process, after which it is found a colloidal stability of MoS₂ in the non-polar solvent, related to the chemical bonding between the molecules and atoms along the sample edges²⁸. In this sense, the edge generation in MoS₂ through techniques assisted by butadiene molecules probably result in systems with those molecules adsorbed in MoS₂ bulk and edge sites. Thus, having in mind eventual future nanotechnology applications, it is essential to know some fundamental characteristics such as (i) the most likely adsorption sites and the corresponding stable geometries; (ii) Details of the adsorption mechanism (physisorption/chemisorption, binding energy, etc.); (iii) and the role of butadiene molecules in the electronic transport of MoS₂. The main objective of our work is to shed light in those questions. Molecules and atoms absorbed in different 2d-materials studies provide excellent candidates for gas sensor and H-storage devices as is the case of phosphorene and MoS₂ itself^{29–34}. The binding energies presented in previous reports for absorbed atoms and molecules in MoS₂ are comparable with ours results. Furthermore, Mo-terminated edges have been demonstrated to be more active, *i.e.* more energetically favorable, when compared to the S-termination, which is in line with our findings^{35,36}.

In this work, we investigate the adsorption of butadiene molecules in MoS₂ nanoribbons and its influence in the electronic transport properties. We employ nanoribbons with zigzag edge termination (ZZNRs). Our results were obtained with a methodology based on *ab initio* density functional theory (DFT) calculations, combined with the recursive non-equilibrium Green's function techniques, taking into account the effects of disorder and different coverages. Such a methodology allows a full description of the transport properties of large-scale devices. We show that butadiene molecules adsorbed on the central region of the nanoribbons do not change the electric current, whereas adsorption at the edge sites (which are the energetically preferable ones) suppresses the charge flowing through the metallic edge states due to a backscattering process. Our findings demonstrate that the low energy edge transport channels of TMDCs are highly susceptible to the adsorption of molecules. Thus, the route used to reduce the dimensionality of TMDCs will have great influence in the transport properties.

2 Computational details

An accurate atomistic simulation of MoS₂ with edges and adsorbed molecules requires a methodology with a great prediction capability, which is the case of the first-principle calculations based on DFT^{37,38} we used. The spin-polarized local-density-approximation (LDA)³⁷ is used for the Exchange-correlation functional. We perform all geometry optimizations with the PAW approach, as implemented in the vienna *ab-initio* simulation package (VASP)^{39,40}. In these calculations, we employ 400 eV for the plane-wave expansion cutoff, a force criterion of 0.01 eV/Å, and sample the reciprocal space with 10 \vec{k} -points along the periodic direction of our nanoribbons.

For the electronic transport calculations, we employ a methodology that couples NEGF techniques to DFT calculations. This methodology considers a central scattering region sandwiched be-

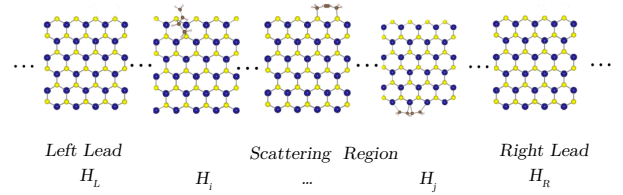


Fig. 1 Schematic representation of the building blocks used to construct the large scale Hamiltonian.

tween the left and right electrodes. We calculated the electric current I in the ballistic approach by the Landauer formula:⁴¹

$$I = \frac{e}{\hbar\pi} \int_{-\infty}^{+\infty} T(E) [f_{FD}(E - \mu_L) - f_{FD}(E - \mu_R)] dE \quad (1)$$

e is the elementary charge, \hbar the reduced Planck's constant, f_{FD} the Fermi-Dirac distribution, E the energy of the charge carrier passing through the system, and $\mu_{L(R)}$ the chemical potential of the left (right) electrode.

$T(E)$ is the transmission probability function, which we evaluate from DFT calculations using the Kohn-Sham Hamiltonian, as described in Refs.⁴² and⁴³. Once sparse matrices are necessary to apply this methodology, it is mandatory to adopt a localized basis set to expand the Kohn-Sham orbitals. This methodology was successfully used to investigate the transport properties of graphene-like materials^{44,45}. Furthermore, to take into account the effects of disorder in large scale systems, the methodology presented in Refs.⁴⁶ and⁴⁷ are employed. The Hamiltonian used to generate the $T(E)$ in a large scale system can be written by:

$$H = \begin{pmatrix} H_L & H_C & 0 & \dots & 0 \\ H_C^\dagger & H_i & H_C & 0 & \vdots \\ 0 & 0 & \ddots & \vdots & 0 \\ \vdots & \vdots & H_C^\dagger & H_j & H_C \\ 0 & \dots & 0 & H_C^\dagger & H_R \end{pmatrix} \quad (2)$$

We show the geometric interpretation of the equation (1) in Fig. 1. H_i and H_j are matrix elements of parts of the scattering region and each one represents either pristine sectors, or fragments of the system containing defects, adsorbed molecules, or any other perturbation. In our work, we constructed the central region by either pristine fragments or nanoribbon sectors with butadiene adsorbed in various adsorption sites. Building blocks randomly positioned along the transport direction are used to construct the scattering region. H_C is the coupling matrix, and we guarantee the same H_C between all building blocks including buffer layers in the geometries. $H_{L(R)}$ are the Hamiltonians of the left and right electrodes.

We calculate the matrix elements of each building block H_i and the coupling matrix H_C via standard DFT calculations. For this purpose, we employ a localized basis set approach as implemented in the SIESTA code. We used a cutoff energy of 250 Ry to defined the mesh size in the real space.

Nanoribbons with 6 (and 12 in few cases) zigzag lines from one edge to the other are used to generate our results. Buffer layers of two unit cells are used to ensure the same coupling term H_C between all building blocks. The pristine blocks and the electrodes have two unit cells along the transport direction, whereas the blocks with adsorbed molecules have seven unit cells. We use a vacuum of 20 Å to separate the periodic images of the nanoribbons.

3 Results

To present our results, we first discuss the structural and energetic properties, in the section 3.1. Subsequently, the transport properties including the disorder effects are shown, in section 3.2.

3.1 Structural and energetic properties

3.1.1 Pristine nanoribbon.

First of all, we focus on the band structure of a TMDC nanoribbon with six zigzag lines, depicted in the left panel of Fig. 2 (a). Its metallic behavior is clear from the bands crossing the Fermi level (which is set at zero). Starting from the previously converged density matrix, we made a Wannier interpolation⁴⁸, using an increased 1x30x1 k-point grid with 30 bands selected such that this set reproduce the band structure for the states surrounding the Fermi level, in particular, the states with pronounced dispersion which will be shown to live at the edges. In this manner, the required construction of the overlap and projections matrices was done by internal routines developed by SIESTA using for this purpose previously selected Mo and S orbitals as an initial basis set. In order to obtain an accurate description in terms of these Wannier functions, this representation must converge to that of one that represents a maximally localized set. Once the above procedure is performed we arrive to the localized orbitals depicted at Fig2 in (b), where the enumerated bands are represented along the edges of the nanoribbon. It is worth to note the edge localization of the metallic states, indicating that the edges of the ribbons are the most active regions for the charge transport. Furthermore, the zigzag nanoribbons edges are not symmetrical. One side has a Mo-rich termination, whereas the other side has a S-rich termination. Such asymmetry is reflected in the band structure.

3.1.2 Adsorption of butadiene on MoS₂ nanoribbons.

With the assumption that transport will take place along the edges, which is more likely given the results obtained so far, we proceed to find the configurations of butadiene molecules adsorbed on MoS₂ nanoribbons. We start from a selected group of configurations and performed a structural optimization of each configuration. With the optimized geometry we calculated the configuration binding energy (E_B), which is given by:

$$E_B = E_{Mol.+MoS_2} - (E_{Mol.} + E_{MoS_2}), \quad (3)$$

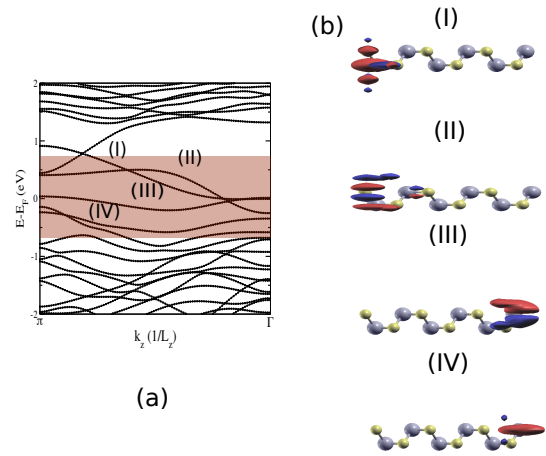


Fig. 2 MoS₂ NR's band structure(a) and (b) projected Wannier states on the pristine structure. The plot shows how are localized along the edges those states leaving in an energy window containing the Fermi level (around ± 0.5 eV). The two different colors represent the positive(red) and negative(blue) real amplitudes for each Wannier orbital.

where $E_{Mol.+MoS_2}$, E_{MoS_2} and $E_{Mol.}$ are the total energies of the butdiene molecule adsorbed, in a given configuration, on MoS₂, MoS₂ nanoribbon and isolated butadiene molecule, respectively. The resulting non-equivalent configurations are showed in Fig. 3. Probably there are many other adsorption configurations. However, the set of structures presented above is a good sample of possibilities to investigate the transport properties once we considered bulk and edge adsorption sites (on both sides of the ribbon).

Table 1 presents the binding energies for our sample adsorption geometries. Our results showed that the two most stable configurations has the molecule bonded adsorbed on the Mo-rich edge. In addition to these configurations, other four adsorption sites with the butadiene molecules attached to the S-rich border are considered, including a particular case where the molecule sits just in-between the edges above the ribbon. These results are in agreement with the charge transfer plot, presented in the Fig. 4, where our zero binding energy reference is characterized by a broader accumulation region along the edge.

Finally, the molecule adsorbed at the central region of the ribbon (configuration 7) has the highest binding energy among all configurations, indicating an energetic preference for edge adsorption. However, its absolute value (0.17 eV) is not small when compared to other systems⁴⁹, indicating a relatively strong interaction between butadiene molecules and the MoS₂ nanoribbon for any one of the investigated configurations.

3.2 Transport properties

3.2.1 Pristine nanoribbon.

In this section, we discuss the transport properties of pristine ZZNRS of TMDCs. To generate the results presented here we employ a single block of pristine nanoribbon as the scattering region. In Fig. 5 we present the source-drain electric current as a function of the bias voltage. Nanoribbons with 6 and 12 zigzag lines

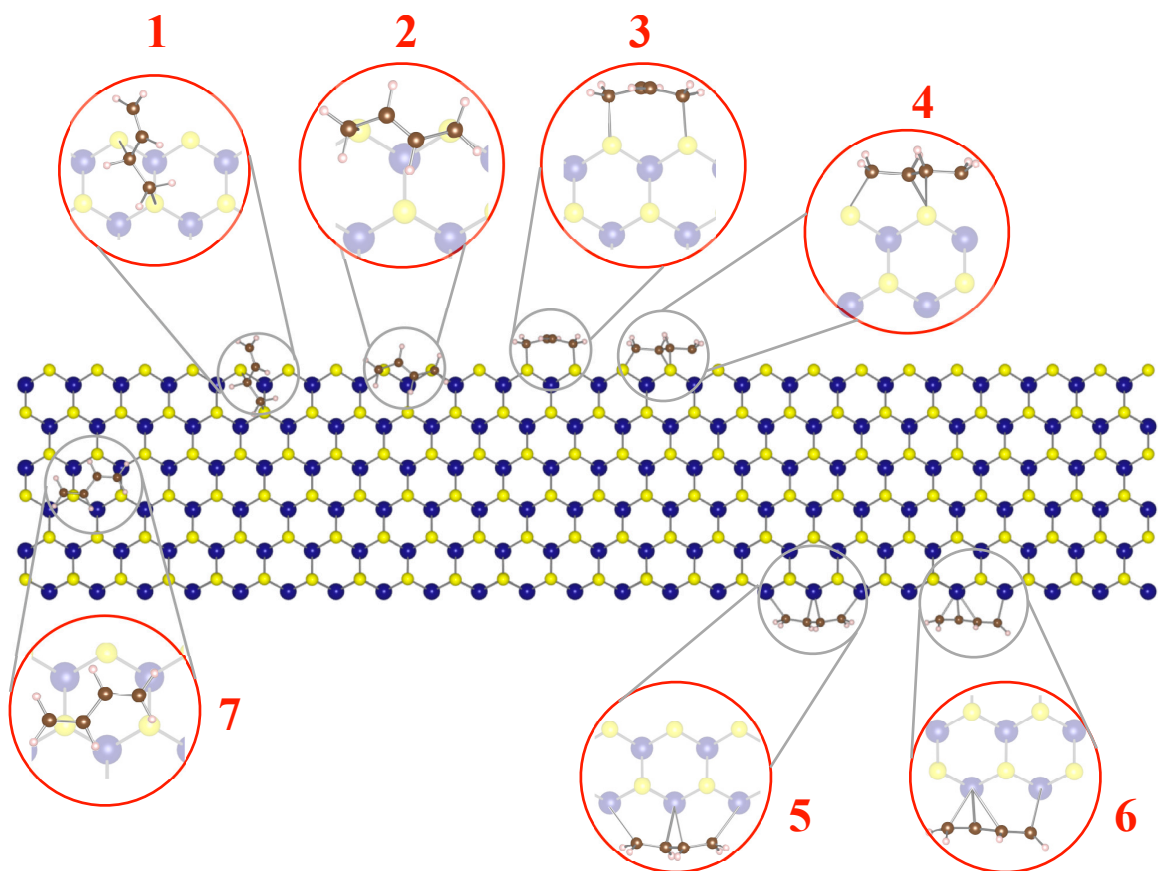


Fig. 3 MoS₂-2H stick-and-ball nanoribbon representation with different butadiene molecule's positions labeled as are represented in table I. This is illustrative representation, since each configuration was calculated in a isolated large supercell.

Table 1 Binding energy for the different butadiene positions in eV/molecule. The negative sign indicated an exothermic process.

Position	Binding energy
1	-0.65
2	-1.53
3	-1.20
4	-0.82
5	-2.82
6	-3.70
7	-0.17

are considered to take into account a width dependence. It is worth to note the NDR for bias voltages between 0.3 and 0.7 V. Such behavior is introduced by the metallic states localized at the edge of the nanoribbons. For bias voltages up to 0.3 V, the edge states of the left and right electrodes are almost aligned in energy, resulting in a high probability for the electrons to cross the scattering region. As the bias increases, the mismatch between edge channels of both electrodes yields to a decreasing in the current, resulting in the NDR behavior. This feature is in agreement with the previous results²⁶.

3.3 Lowest energy configuration

Among the seven adsorption sites aforementioned in section 3.1.2, we demonstrate here the effects in the transport properties of TMDCs ZZNRs generated by a single butadiene molecule

adsorbed in its most stable configuration. To generate these results we consider a scattering region comprised of a single ZZNR block with 7 unit cells and one butadiene molecule adsorbed in the position 6. In this structure, the molecule is located on the Mo-rich edge, and its high binding energy (3.7 eV) demonstrates a strong interaction. Fig. 6, upper panel, shows the local density of states (LDOS), where we've previously shown that those states live along the nanoribbon borders, meaning that states coming from the molecule (inset), interact with the Mo orbitals localized at the edge. As a result, we can see how the transmission curve ($T(E)$) have changed with respect to that one of the pristine case, red and black respectively. Fig. 6, bottom panel, shows $T(E)$. The solid (dashed) line corresponds to configuration 6 (pristine nanoribbon). The butadiene molecule generates a decreasing of $T(E)$ around the Fermi level by almost one transport channel.

3.3.1 Large scale disordered system.

Up to this point, the obtained results suggest the next stage: since ZZNRs present (metallic) edge states in an energy window around the Fermi level, what is the influence in the transport properties if butadiene molecules used in the exfoliation process anchor at the edges of large-scale ZZNRs? At first glance, these interactions will change the electronic structure, and consequently the electronic transport, as indicated in the previous section. The chemical rearrangement experienced by the sample could be related to the existence of quasi-localized states, acting as source

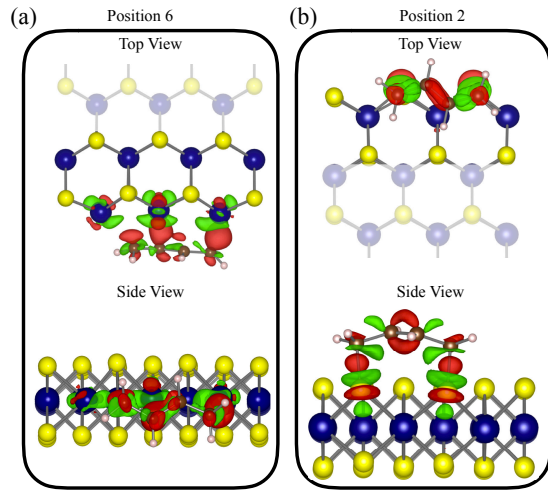


Fig. 4 Butadiene-MoS₂ charge transfer. The butadiene molecule is located at the Mo (a) and S (b) termination side. We considered the lowest energy configuration on each termination, according to table 1. The green (red) isosurfaces represents accumulation (depletion) of charge. An isosurface of 0.008 ($e/\text{Å}^3$) is considered.

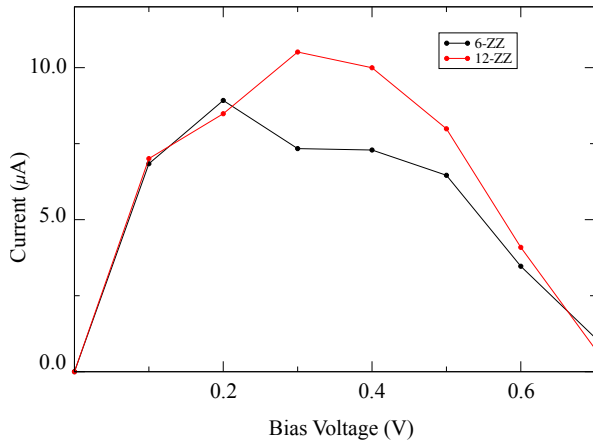


Fig. 5 Current as a function of Bias voltage for 6 and 12 zigzag lines. The Negative Differential Resistance is observed in the same bias energy window as reported previously for both cases and the behaviour of the current for both NR's looks similar as well.

of electron backscattering processes and leading to a drop in the transmission. Another possibility is the presence of stronger localized states which could lead to a different electronic transport trend.

The previous section demonstrates that a single adsorbed molecule already significantly modify the transport properties of TMDC nanoribbons. In this section, we are interested in to understand the effects of several butadiene molecules in large scale nanoribbons. Our results are obtained by using the previous arrangements as building blocks to increase the size of our scattering region along the transport direction, as we've mentioned, this is possible with the application of a decimation process^{46,47}. With this procedure, we obtain the transmission function shown in Fig. 7, where we have different curves for different quantities of molecules attached to the ribbon and are presented as an average over thirty different distributions with the same number

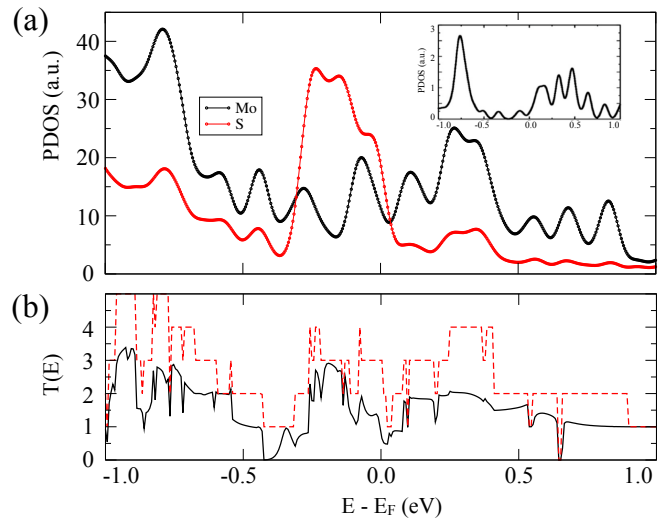


Fig. 6 Projected density of states (PDOS) (a), and transmission coefficients (T) (b), for the most stable configuration (position 6). In (a) the inset shows the PDOS for the molecule in the same energy window used for both PDOS and $T(E)$ while in (b) the dashed red curve is the transmission $T(E)$ for the pristine structure. The Fermi level is set to zero.

of molecules, the dashed line represents the pristine case and the others show how the values of the transmission are getting smaller as the number of molecules becomes larger. The scatter length can be estimated by the following relation

$$L_{Total}(n) = n * L_{Molecule} + (50 - n) * L_{Pristine} \quad (4)$$

Where L_{Total} is the total length of the scattering region, n the number of molecules, $L_{Molecule}$ is the length of a piece of NR with one molecule attached (which is the same for all the molecules) and $L_{Pristine}$ is the length of molecule-free pieces of NR which are used as buffer regions. Having these values, for 5 molecules the total length is of 574.2 Å, a number which increases ranging values up to 1052.7 Å for 30 molecules.

In Fig. 8, we show the current obtained with an applied bias voltage of 0.1 V; again this figure shows a current decreasing with the increase on the number of molecules. In the inset we also show the conductance calculated as an average, given the $T(E)$ we know that if μ represents the chemical potential we can write

$$G(\mu) = \int dE T(E) \frac{df_{FD}(E' - \mu)}{dE'} \Big|_{E'=E}, \quad (5)$$

where the conductance is calculated in units of $2e^2/h$. The observed values obtained for the current are supported by the average conductance curve, which has a decaying behaviour suggesting that butadiene molecules yield to a localization regime once we are working in the nanometer scale.

On the experimental side, processing residues and imperfect electrical contacts play an important role when it comes to determine regimes at which the transport measurements are made^{50,51}. The use of Si/SiO₂ as substrate lead to a localization up to room temperature, which is related to the disorder arising from randomly distributed charges at the interface between the

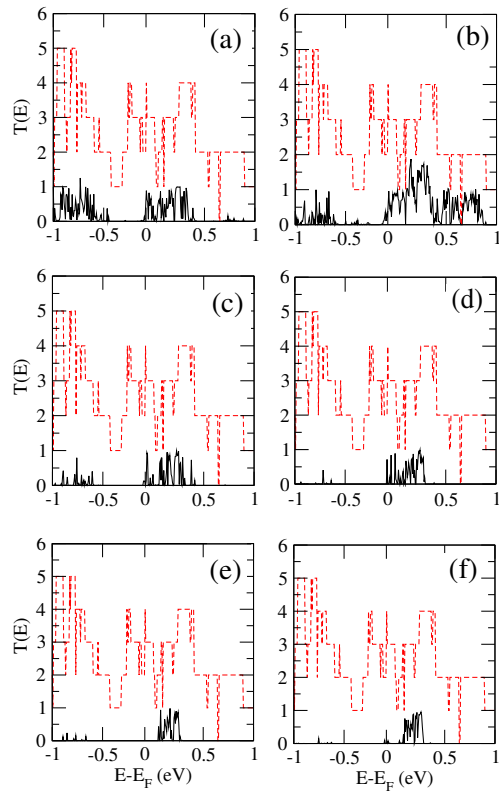


Fig. 7 Transport coefficients for (a) 5, (b) 10, (c) 20, (d) 30, (e) 40 and (f) 50 molecules attached to the NNR (black curves). For sake of comparison we also show the transmission calculated for the pristine structure (red curve). Each of them was calculated under a 0.1 V bias.

sample and substrate, in others words, this suggests that the electronic behaviour could be enhanced by a careful engineering of the substrate made for the sample⁵².

The transport calculations show a correlation between the existence of the quasi-localized states and the decreasing in the transport coefficients, as usual, this has to do with backscattering processes which lead to a suppressed transmission, where is evident how the transmission decreases as there are more molecules attached to the nanoribbon then acting as source of scattering processes^{53–55}. Previous experimental works pointed out the charged impurities and localized states are very important in exfoliated samples, different sources give rise to scattering processes and then it's hard to find an accurate transport mechanism for this cases. The existence of localized states usually makes difficult a ballistic transport but it's been observed that this is possible when the sample is highly doped where band transport can be achieved^{56–58}.

4 Conclusions

In this work, we investigated the influence of butadiene molecules in the transport properties of MoS₂ zig-zag nanoribbons with metallic edge states. Our simulations took into account the effects of disorder and different coverages in large-scale systems ($\approx \mu\text{m}$). Our principal motivation is the experimental use of butadiene molecules in the dimensionality reduction process of MoS₂, re-

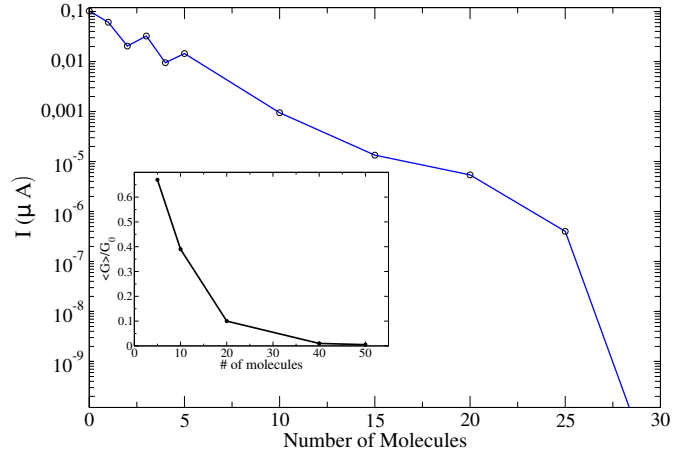


Fig. 8 Current in μA for different number of molecules attached to the NR for an applied bias of 0.1 V, the values are present in a log scale in order to show how the current decreases by orders of magnitude once the number of molecules increases, besides we show how the average conductance $\langle G \rangle / G_0$ (G_0 being the conductance quantum) at the Fermi level decays.

cently published in the literature²⁸. Our results allow to infer that MoS₂ nanoribbons containing adsorbed butadiene molecules lost its metallic behavior due to backscattering process. Such a behavior highly contrasts with pristine TMDCs nanoribbons. Furthermore, the relatively high absolute value for the binding energy indicates that a cleaning process (removing butadiene molecules from MoS₂) is a hard task. Thus, the mechanisms used to reduce the dimensionality of MoS₂ considerably modify its transport properties.

5 Conflict of Interest

The authors declare that there are no conflicts of interest.

6 Acknowledgements

This work was supported by the Brazilian agencies *Fundação de Amparo à Pesquisa do Estado de São Paulo (FAPESP)* (grants 16/14011-2 and 17/02317-2), CAPES and INCT/CNPQ. We would like to acknowledge computing time to the UFABC, and SAMPA group for the computational facilities. The authors also acknowledge the National Laboratory for Scientific Computing (LNCC/MCTI, Brazil) for providing HPC resources of the SDumont supercomputer, which have contributed to the research results reported within this paper. URL: <http://sdumont.lncc.br>

Notes and references

- 1 K. S. Novoselov, A. K. Geim, S. V. Morozov, D. Jiang, Y. Zhang, S. V. Dubonos, I. V. Grigorieva and A. A. Firsov, *Science*, 2004, **306**, 666–669.
- 2 K. S. Novoselov, A. Mishchenko, A. Carvalho and A. H. Castro Neto, *Science*, 2016, **353**, aac9439.
- 3 K. S. Novoselov, A. K. Geim, S. V. Morozov, D. Jiang, M. I.

- Katsnelson, I. V. Grigorieva, S. V. Dubonos and A. A. Firsov, *Nature*, 2005, **438**, 197–200.
- 4 K. S. Kim, Y. Zhao, H. Jang, S. Y. Lee, J. M. Kim, K. S. Kim, J.-H. Ahn, P. Kim, J.-Y. Choi and B. H. Hong, *Nature*, 2009, **457**, 706 EP –.
 - 5 A. A. Balandin, S. Ghosh, W. Bao, I. Calizo, D. Teweldebrhan, F. Miao and C. N. Lau, *Nano Letters*, 2008, **8**, 902–907.
 - 6 L. A. Falkovsky, *Journal of Physics: Conference Series*, 2008, **129**, 012004.
 - 7 A. H. Castro Neto, F. Guinea, N. M. R. Peres, K. S. Novoselov and A. K. Geim, *Rev. Mod. Phys.*, 2009, **81**, 109–162.
 - 8 S. A. Han, R. Bhatia and S.-W. Kim, *Nano Convergence*, 2015, **2**, 17.
 - 9 A. Kormányos, G. Burkard, M. Gmitra, J. Fabian, V. Zólyomi, N. D. Drummond and V. Fal'ko, *2D Materials*, 2015, **2**, 022001.
 - 10 C. Ataca and S. Ciraci, *The Journal of Physical Chemistry C*, 2011, **115**, 13303–13311.
 - 11 X. Qian, J. Liu, L. Fu and J. Li, *Science*, 2014, **346**, 1344–1347.
 - 12 M. Chhowalla, H. S. Shin, G. Eda, L.-J. Li, K. P. Loh and H. Zhang, *Nature Chemistry*, 2013, **5**, 263 EP –.
 - 13 Y. An, J. Jiao, Y. Hou, H. Wang, R. Wu, C. Liu, X. Chen, T. Wang and K. Wang, *Journal of Physics: Condensed Matter*, 2018, **31**, 065301.
 - 14 Y. An, Y. Sun, M. Zhang, J. Jiao, D. Wu, T. Wang and K. Wang, *IEEE Transactions on Electron Devices*, 2018, **65**, 4646–4651.
 - 15 Y. An, Y. Sun, J. Jiao, M. Zhang, K. Wang, X. Chen, D. Wu, T. Wang, Z. Fu and Z. Jiao, *Organic Electronics*, 2017, **50**, 43 – 47.
 - 16 M. Zhang, Y. An, Y. Sun, D. Wu, X. Chen, T. Wang, G. Xu and K. Wang, *Phys. Chem. Chem. Phys.*, 2017, **19**, 17210–17215.
 - 17 Y. An, M. Zhang, D. Wu, Z. Fu and K. Wang, *J. Mater. Chem. C*, 2016, **4**, 10962–10966.
 - 18 Y. An, J. Jiao, Y. Hou, H. Wang, D. Wu, T. Wang, Z. Fu, G. Xu and R. Wu, *Phys. Chem. Chem. Phys.*, 2018, **20**, 21552–21556.
 - 19 X. Chia, A. Ambrosi, Z. Sofer, J. Luxa and M. Pumera, *ACS Nano*, 2015, **9**, 5164–5179.
 - 20 G. Zhang and Y.-W. Zhang, *J. Mater. Chem. C*, 2017, **5**, 7684–7698.
 - 21 T. Akama, W. Okita, R. Nagai, C. Li, T. Kaneko and T. Kato, *Scientific Reports*, 2017, **7**, 11967.
 - 22 H. Pan and Y.-W. Zhang, *J. Mater. Chem.*, 2012, **22**, 7280–7290.
 - 23 C. Ataca, H. Sahin and S. Ciraci, *The Journal of Physical Chemistry C*, 2012, **116**, 8983–8999.
 - 24 H. Liu, A. T. Neal and P. D. Ye, *ACS Nano*, 2012, **6**, 8563–8569.
 - 25 Y. Yoon, K. Ganapathi and S. Salahuddin, *Nano Letters*, 2011, **11**, 3768–3773.
 - 26 Y. An, M. Zhang, H. Da, Z. Fu, Z. Jiao and Z. Liu, *Journal of Physics D: Applied Physics*, 2016, **49**, 245304.
 - 27 J. N. Coleman, M. Lotya, A. O'Neill, S. D. Bergin, P. J. King, U. Khan, K. Young, A. Gaucher, S. De, R. J. Smith, I. V. Shvets, S. K. Arora, G. Stanton, H.-Y. Kim, K. Lee, G. T. Kim, G. S. Duesberg, T. Hallam, J. J. Boland, J. J. Wang, J. F. Donegan, J. C. Grunlan, G. Moriarty, A. Shmeliov, R. J. Nicholls, J. M. Perkins, E. M. Grieveson, K. Theuvsissen, D. W. McComb, P. D. Nellist and V. Nicolosi, *Science*, 2011, **331**, 568–571.
 - 28 R. H. Gonçalves, R. Fiel, M. R. S. Soares, W. H. Schreiner, C. M. P. Silva and E. R. Leite, *Chemistry - A European Journal*, 2015, **21**, 15583–15588.
 - 29 Q. Yue, Z. Shao, S. Chang and J. Li, *Nanoscale Research Letters*, 2013, **8**, 425.
 - 30 S. Yang, D. Li, T. Zhang, Z. Tao and J. Chen, *The Journal of Physical Chemistry C*, 2012, **116**, 1307–1312.
 - 31 K. K. Ghuman, S. Yadav and C. V. Singh, *The Journal of Physical Chemistry C*, 2015, **119**, 6518–6529.
 - 32 Y. Cai, Q. Ke, G. Zhang and Y.-W. Zhang, *The Journal of Physical Chemistry C*, 2015, **119**, 3102–3110.
 - 33 S. J. Rodríguez and E. A. Albanesi, *Phys. Chem. Chem. Phys.*, 2019, **21**, 597–606.
 - 34 V. Shukla, J. Wärnå, N. K. Jena, A. Grigoriev and R. Ahuja, *The Journal of Physical Chemistry C*, 2017, **121**, 26869–26876.
 - 35 M. Huang and K. Cho, *The Journal of Physical Chemistry C*, 2009, **113**, 5238–5243.
 - 36 C. Ataca, H. Şahin, E. Aktürk and S. Ciraci, *The Journal of Physical Chemistry C*, 2011, **115**, 3934–3941.
 - 37 P. Hohenberg and W. Kohn, *Physical Review*, 1964, **136**, B864–B871.
 - 38 G. R. Schleder, A. C. M. Padilha, C. M. Acosta, M. Costa and A. Fazzio, *Journal of Physics: Materials*, 2019. <https://doi.org/10.1088/2515-7639/ab084b>.
 - 39 G. Kresse and J. Furthmüller, *Comput. Mater. Sci.*, 1996, **6**, 15–50.
 - 40 G. Kresse and J. Furthmüller, *Phys. Rev. B*, 1996, **54**, 11169–11186.
 - 41 R. Landauer, *The Philosophical Magazine: A Journal of Theoretical Experimental and Applied Physics*, 1970, **21**, 863–867.
 - 42 F. D. Novaes, A. A. J. R. d. Silva and A. Fazzio, *Brazilian Journal of Physics*, 2006, **36**, 799 – 807.
 - 43 M. Brandbyge, J.-L. Mozos, P. Ordejón, J. Taylor and K. Stokbro, *Phys. Rev. B*, 2002, **65**, 165401.
 - 44 M. P. Lima, A. J. R. da Silva and A. Fazzio, *Phys. Rev. B*, 2011, **84**, 245411.
 - 45 M. P. Lima, A. Fazzio and A. J. R. da Silva, *IEEE Electron Device Letters*, 2018, **39**, 1258–1261.
 - 46 A. R. Rocha, M. Rossi, A. Fazzio and A. J. R. da Silva, *Phys. Rev. Lett.*, 2008, **100**, 176803.
 - 47 A. R. Rocha, M. Rossi, A. J. R. da Silva and A. Fazzio, *Journal of Physics D: Applied Physics*, 2010, **43**, 374002.
 - 48 A. A. Mostofi, J. R. Yates, G. Pizzi, Y.-S. Lee, I. Souza, D. Vanderbilt and N. Marzari, *Computer Physics Communications*, 2014, **185**, 2309 – 2310.
 - 49 O. Leenaerts, B. Partoens and F. M. Peeters, *Phys. Rev. B*, 2008, **77**, 125416.
 - 50 V. K. Sangwan and M. C. Hersam, *Annual Review of Physical Chemistry*, 2018, **69**, 299–325.
 - 51 S. Bhandari, K. Wang, K. Watanabe, T. Taniguchi, P. Kim and

- R. M. Westervelt, *Journal of Physics: Conference Series*, 2017, **864**, 012031.
- 52 S. Ghatak, A. N. Pal and A. Ghosh, *ACS Nano*, 2011, **5**, 7707–7712.
- 53 B. Biel, X. Blase, F. m. c. Triozon and S. Roche, *Phys. Rev. Lett.*, 2009, **102**, 096803.
- 54 I. Deretzis, G. Fiori, G. Iannaccone and A. La Magna, *Phys. Rev. B*, 2010, **81**, 085427.
- 55 A. López-Bezanilla, F. Triozon, S. Latil, X. Blase and S. Roche, *Nano Letters*, 2009, **9**, 940–944.
- 56 B. W. H. Baugher, H. O. H. Churchill, Y. Yang and P. Jarillo-Herrero, *Nano Letters*, 2013, **13**, 4212–4216.
- 57 H. Schmidt, S. Wang, L. Chu, M. Toh, R. Kumar, W. Zhao, A. H. Castro Neto, J. Martin, S. Adam, B. Özyilmaz and G. Eda, *Nano Letters*, 2014, **14**, 1909–1913.
- 58 D. Jariwala, V. K. Sangwan, D. J. Late, J. E. Johns, V. P. Dravid, T. J. Marks, L. J. Lauhon and M. C. Hersam, *Applied Physics Letters*, 2013, **102**, 173107.